Universiteit
Leiden
The Netherlands

# Unravelling Heterodyne Force Microscopy

Verbiest, G.J.

**Citation**
Verbiest, G. J. (2013, November 19). *Unravelling Heterodyne Force Microscopy*. *Casimir PhD Series*. Retrieved from https://hdl.handle.net/1887/22238

| | |
|---|---|
| Version: | Not Applicable (or Unknown) |
| License: | Leiden University Non-exclusive license |
| Downloaded from: | https://hdl.handle.net/1887/22238 |

**Note:** To cite this publication please use the final published version (if applicable).

Cover Page

Universiteit Leiden


The handle http://hdl.handle.net/1887/22238 holds various files of this Leiden University dissertation

**Author:** Verbiest, Gerard Jan
**Title:** Unravelling heterodyne force microscopy
**Issue Date:** 2013-11-19

# CHAPTER 5

## Beating beats Nonlinear Mixing in Heterodyne Force Microscopy

*Heterodyne detection schemes are widely used to detect high frequency signals, which are unmeasurable with conventional techniques. Although counterintuitive, we demonstrate that beating, which is a linear effect and does not generate a heterodyne signal, dominates the heterodyne signal that is generated by nonlinear mixing, if the nonlinearity of the system is of higher order than quadratic. We confirm our results experimentally using Heterodyne Force Microscopy, which is a typical example of a system with a nonquadratic nonlinearity. Our study implies that results of previously reported heterodyne measurements, in which the nonlinearity is of higher order than quadratic, may need to be reconsidered.*

Most of this chapter is submitted for publication in Nature Physics

## 5.1 Introduction

There are many periodic processes with such a high frequency that they are difficult to measure experimentally. A solution is the application of a heterodyne detection scheme, as it down-converts the high frequency signal to a lower, easily measurable frequency by mixing it with a reference signal. This enables the quantification of the amplitude, the phase, and the frequency modulation of the original, high frequency signal. A well-known example of a heterodyne detector is the radio. Heterodyne detection is also widely used in optics, in quantum devices, in the detection of nuclear magnetic resonance, in microwave detection, and even in the search for gravitational waves [60–65].

Recently, heterodyne detection was implemented in Atomic Force Microscopy, called Heterodyne Force Microscopy, see [2–5], to enable the non-destructive imaging *below* a surface with nanometer resolution [6–14, 53]. The subsurface information is contained in an ultrasonic sound wave that travelled through the sample and has a frequency $\omega_s$ of several MHz. To detect this signal, a Heterodyne Force Microscope (HFM) makes use of the nonlinear interaction between the cantilever's tip and the sample such that a heterodyne signal at a lower difference frequency $\omega_{\text{diff}} = |\omega_s - \omega_t|$ is generated, if one excites also the cantilever with a frequency $\omega_t$ that deviates slightly from the sample frequency $\omega_s$, see Fig. 5.1. Despite the successful application of Heterodyne Force Microscopy, the generation of the heterodyne signal is not well understood, which allows only qualitative interpretations.

In this chapter we demonstrate that beating, which is ought to occur only with a linear interaction term, dominates also the heterodyne signal generated by nonlinear mixing. The specific characteristics of the nonlinear interaction that define the mixer, determine the sensitivity for beating. On the example of Heterodyne Force Microscopy, we show that beating is important for all mixers that have a nonlinearity of higher order than quadratic.

## 5.2 Beating and Nonlinear Mixing

Beating and mixing have each a unique Fourier spectrum. Beating occurs with a linear mixer such that one sums over two (or more) harmonic excitations, see upper panel of Fig. 5.2A. The result (black line) oscillates at an ultrasonic frequency $\omega_h$ between $\omega_s$ and $\omega_t$ and *appears* also to oscillate at the difference frequency $\omega_{\text{diff}}$ (red lines). However, as the Fourier spectrum of the time trace only shows the two original frequencies $\omega_s$ and $\omega_t$, no signal is detectable at the difference frequency $\omega_{\text{diff}}$. Mixing, see lower panel of Fig. 5.2A, occurs with

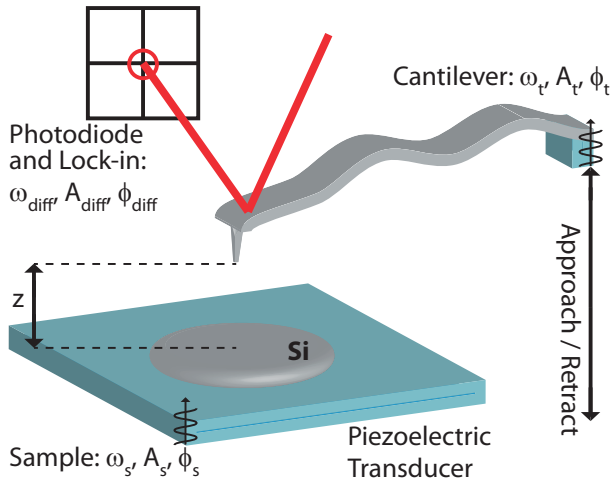


Figure 5.1: HFM excitation scheme: the Silicon sample vibrates with amplitude $A_s$ and phase $\phi_s$ at a frequency $\omega_s$, while the tip vibrates with $A_t$ and $\phi_t$ at $\omega_t$. Using an optical beam method and a lock-in, we detected the amplitude $A_{\text{diff}}$ and phase $\phi_{\text{diff}}$ of the diference frequency $\omega_{\text{diff}} = |\omega_s - \omega_t|$. The tip-sample distance $z$ was varied by moving the cantilever towards the surface (approach) and out again (retract).

a nonlinear interaction and is usually the product of two harmonic excitations. The result really oscillates at the difference frequency (red line) and the sum frequency (black line). In contrast to beating, the Fourier spectrum of the time trace shows the difference and the sum frequency, but *not* the frequencies of the two, original harmonic excitations. Therefore, beating and mixing are two intrinsically different effects that are classified by the type of interaction and their Fourier analysis.

The typical excitation scheme used in a HFM is shown in Fig. 5.1. The sample vibrates with amplitude $A_s$ and phase $\phi_s$ at a frequency $\omega_s$. At the same time, the cantilever vibrates with amplitude $A_t$ and phase $\phi_t$ at a frequency $\omega_t$. The ultrasonic excitation frequencies $\omega_s$ and $\omega_t$ are chosen well *above* the first resonance of the cantilever, while their frequency difference $\omega_{\text{diff}}$ is *below* the first resonance. As a consequence, the cantilever is not able to follow the ultrasonic motion of the sample, but it is able to follow the heterodyne signal generated at the difference frequency $\omega_{\text{diff}}$.

Figure 5.2B depicts the heterodyne signal generation in a HFM. The sum of the high frequency motion of both the cantilever $A_t \cos(\omega_t t)$ and the sample $A_s \cos(\omega_s t)$ results in beating of the tip-sample distance. Note that both the amplitude of the ultrasonic tip motion $A_t$ and the amplitude of the ultrasonic sample motion $A_s$ are assumed to be *constant* for all tip-sample distances $z$.

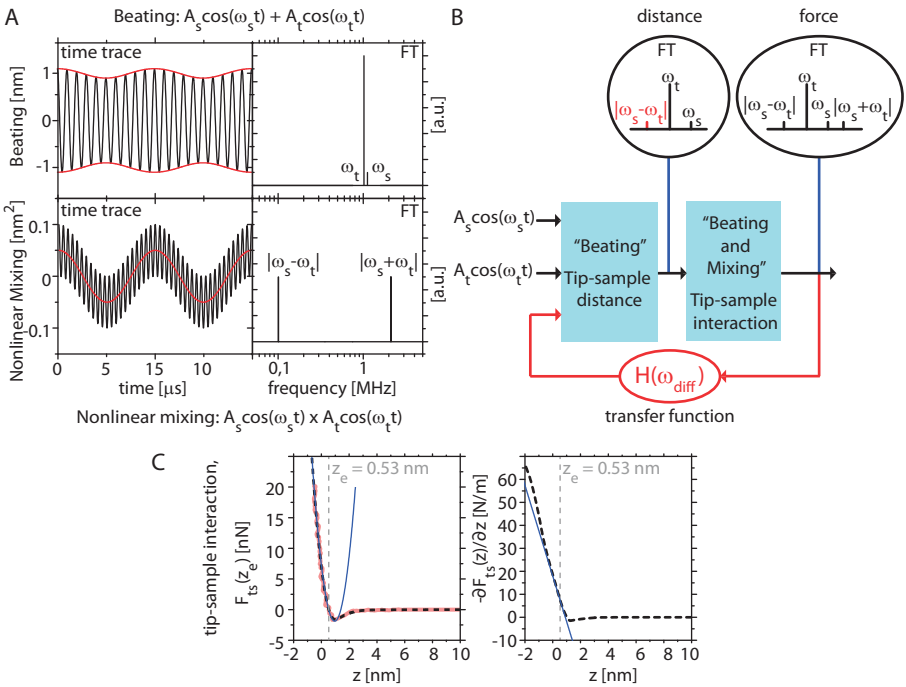


Figure 5.2: (A) Beating versus nonlinear mixing with $\omega_s = 1.1$ MHz, $\omega_t = 1$ MHz, $A_s = 0.1$ nm, and $A_t = 1$ nm. Beating is the sum of two harmonic functions (upper panel): the Fourier spectrum (FT) contains *only* the two original frequencies $\omega_s$ and $\omega_t$. Nonlinear mixing is the product of two harmonic functions (lower panel): the FT contains *only* the two nonlinear frequencies $|\omega_s - \omega_t|$ and $|\omega_s + \omega_t|$. (B) The tip-sample distance is the sum of the ultrasonic motion of the cantilever $A_t \cos(\omega_t t)$ and the sample $A_s \cos(\omega_s t)$, which results in beating. The nonlinear tip-sample interaction generates a drive force at the sum and the difference frequency, which is fed back into the tip-sample distance via the transfer function $H(\omega_{\text{diff}})$ of the cantilever (red arrow). The FTs show the frequencies present before and after the mixer that describes the tip-sample interaction. (C) The tip-sample interaction as a function of the distance $z$ (left panel): obtained from the experiment (red), as used in the analytical calculation (dashed black), and a second order approximation around $z_e = 0.53$ (blue). Please note that $F_{ts}(z = 0) \neq 0$ per definition. The derivative of the tip-sample interaction as a function of the distance $z$ (right panel): as used in the analytical calculation (dashed black) and the second order approximation around $z_e = 0.53$ (blue). The blue line is only a good approximation of $F_{ts}$ near $z = z_e = 0.53$.

This nontrivial assumption has been suggested [5,53] and, in addition, recently predicted theoretically as well as confirmed experimentally (see Chaps. 3 and 4 as well as [42,52]). The tip-sample distance is the input of the mixer that describes the nonlinear tip-sample interaction. This mixer generates a drive force at the difference frequency, which results in a *real* motion of the cantilever. Therefore, the force is fed back into the tip-sample distance via the transfer function of the cantilever, which is characterized by $H(\omega_{\text{diff}})$. We address the general case without feedback mechanism below and show that beating still gives corrections to the heterodyne signal.

## 5.3 Results and Discussion

To derive an expression for the signal at the difference frequency, we need a description of the tip-sample distance $z$ that has a static offset $z_b$ given by the position of the cantilever's base. To account for a possible bending of the cantilever, we include the deflection $\delta$ (which is a function of the spring constant of the cantilever) in addition to the ultrasonic motion of both the cantilever and the sample. Finally, we add the feedback term, see Appx. 5.A.1, that accounts for the motion of the cantilever at the difference frequency $\omega_{\text{diff}}$.

$$z = z_b + \delta + A_{\text{diff}} \cos(\omega_{\text{diff}} t + \phi_{\text{diff}}) + A_s \cos(\omega_s t + \phi_s) + A_t \cos(\omega_t t + \phi_t) \quad (5.1)$$

To enable a proper comparison between the simulations and the experiments, we subtract an offset in $z_b$ such that $z_b = 0$, if the deflection $\delta = 0$ during the approach cycle of the cantilever to the surface. This is exactly the point, at which the *effective* interaction (contact force) $F_c$ on the tip changes sign from an attractive interaction to a repulsive interaction. Equation 5.1 is used in the tip-sample interaction $F_{ts}(z)$ to find the effective drive force on the cantilever at the difference frequency. This can be done in two ways: either one makes, as usual, a *second* order Taylor expansion of the tip-sample interaction $F_{ts}$ around the equilibrium position $z_e = z_b + \delta$ of the cantilever, or one first uses beating to rewrite the high frequency motion of both the tip and the sample as a motion at a high frequency $\omega_h$ with amplitude $A_h = \sqrt{A_s^2 + A_t^2}$ and an amplitude modulated term at frequency $\omega_h$, before making a *linear* expansion of the tip-sample interaction $F_{ts}$ around a *time varying* equilibrium position of the cantilever. The first method, referred to as *standard nonlinear mixing*, is valid only for second order (quadratic) interactions, whereas the latter, referred to as *beating and mixing*, is valid for any type of interaction. The derivations and validities of both methods are described in detail in Appx. 5.A. Next to the fact that "beating and mixing" is the more general theoretical description, additional proof for "beating and mixing" is found in our HFM experiments, which we discuss below.

Let us now compare the solutions of both methods, in which the amplitude

$A_{\text{diff}}$ and the phase $\phi_{\text{diff}}$ of the heterodyne signal (Tab. 5.1: Eq. 5.2) and the static deflection $\delta$ of the cantilever (Tab. 5.1: Eq. 5.3) are determined by three parameters: $I_0$ denotes the average tip-sample interaction, $I_1$ denotes an effective tip-sample spring, and $I_2$ represents an effective mixing term. In the "standard nonlinear mixing" solution, $I_1$ and $I_2$ are determined by the values of the first and the second derivative of the tip-sample interaction at the equilibrium position $z_e$. In contrast, the "beating and mixing" solution takes explicitly into account the high frequency motion and, therefore, the derivative of the tip-sample interaction at *all* tip-sample distances between $z_e$ and $z_e \pm A_h$. This description holds as long as $A_s \cdot A_t$ is smaller than $A_h^2$. The three parameters $I_0$, $I_1$ and $I_2$ become weighted integrals of $F_{ts}$ and $\partial F_{ts}/\partial z$. If the nonlinear mixer is purely quadratic, the integrals reduce to the values for $I_0$, $I_1$ and $I_2$ of the solution of "standard nonlinear mixing" (see Appx. 5.A.2). Therefore, the "beating and mixing" solution is required for all interactions that cannot be approximated with a quadratic function.

The tip-sample interaction in Heterodyne Force Microscopy deviates significantly from a quadra-tic behavior. This becomes evident from the left panel of Fig. 5.2C, in which we show $F_{ts}$ obtained from the experiment (red), $F_{ts}$ as used in the analytical calculation (dashed black), and the quadratic interaction or second order approximation of $F_{ts}$ around $z = z_e = 0.53$ nm (blue). Although the quadratic interaction is a good approximation of the tip-sample interaction close to $z_e = 0.53$ nm, this approximation clearly fails at a tip-sample distance of, e.g., $z = z_e = 1.53$ nm. This is even worse for the first derivative of the tip-sample interaction, which is shown in the right panel of Fig. 5.2C. Therefore, "standard nonlinear mixing" does not describe the heterodyne signal generation in a HFM: the tip-sample interaction is not quadratic over a $z$ range equal to the typical ultrasonic vibration amplitude $A_h$ of 1 nm.

To plot the difference signal analytically, we need the inverse transfer function of the cantilever, which is characterized by its absolute value $|H^{-1}(\omega_{\text{diff}})|$ and its phase shift $\Lambda$. If the cantilever approaches the sample, the tip-sample interaction acts on the free end of the cantilever and causes a shift in resonance frequency, a corresponding phase shift, and a change in mode shape (see Appx. 5.B).

To confirm experimentally that "beating and mixing" is important in Heterodyne Force Microscopy, we measured both the amplitude of the heterodyne signal $A_{\text{diff}}$ and the deflection $\delta$ as a function of the tip-sample distance (defined by the cantilever's base position $z_b$), see Fig. 5.3A. The hysteresis is the result of the detection via a lock-in. If we would have measured significantly slower, there would be no hysteresis. We used a 2 N/m cantilever, which has its first resonance frequency around 70 kHz. The sample was a freshly cleaned Silicon wafer. We obtained an analytical description of the tip-sample interaction by fitting the Derjaguin-Muller-Toporov model [23] and $I_0$ to the experimental

$$A_{\mathrm{diff}} e^{\mathrm{i}\phi_{\mathrm{diff}}} = \frac{A_s A_t}{\sqrt{A_s^2 + A_t^2}} \frac{I_2 e^{\mathrm{i}(\phi_s - \phi_t)}}{|H^{-1}(\omega_{\mathrm{diff}})| e^{\mathrm{i}\Lambda} - I_1} \tag{5.2}$$

$$\delta = I_0 / k \tag{5.3}$$

| **Standard nonlinear Mixing** | **Beating and Mixing** |
|---|---|
| $I_0 = F_{ts}(z_b + \delta)$ | $I_0 = \frac{1}{\pi} \int_{-1}^{1} F_{ts}\left(z_b + \delta + \sqrt{A_s^2 + A_t^2}u\right) \frac{du}{\sqrt{1-u^2}}$ |
| $I_1 = \frac{\partial F_{ts}}{\partial z}(z_b + \delta)$ | $I_1 = \frac{1}{\pi} \int_{-1}^{1} \frac{\partial F_{ts}}{\partial z}\left(z_b + \delta + \sqrt{A_s^2 + A_t^2}u\right) \frac{du}{\sqrt{1-u^2}}$ |
| $I_2 = \frac{1}{2}\sqrt{A_s^2 + A_t^2} \frac{\partial^2 F_{ts}}{\partial z^2}(z_b + \delta)$ | $I_2 = \frac{1}{\pi} \int_{-1}^{1} \frac{\partial F_{ts}}{\partial z}\left(z_b + \delta + \sqrt{A_s^2 + A_t^2}u\right) \frac{udu}{\sqrt{1-u^2}}$ $= \frac{\sqrt{A_s^2 + A_t^2}}{2\pi} \int_{-1}^{1} \frac{\partial^2 F_{ts}}{\partial z^2}\left(z_b + \delta + \sqrt{A_s^2 + A_t^2}u\right) \sqrt{1-u^2}du$ |

Table 5.1: The general solutions, see Appx. 5.A, for the generated heterodyne signal (Eq. 5.2), which is characterized by $I_1$ and $I_2$, and the static deflection, (Eq. 5.3), which is characterized by $I_0$. The parameters for "standard nonlinear mixing" are given in the first column, and for "beating and mixing" in the second column. If the tip-sample interaction $F_{ts}$ is purely quadratic, the parameters of both solutions become equal. "Beating and mixing" explicitly takes into account the high frequency motion and, therefore, the values of $F_{ts}$ and $\partial F_{ts}/\partial z$ at *all* tip-sample distances between $z_e$ and $z_e \pm A_h$, in which $A_h = \sqrt{A_s^2 + A_t^2}$.

deflection $\delta$ (see Appx. 5.D). The cantilever was excited at 2.87 MHz with an amplitude of 0.96 nm, while the sample was excited such that $\omega_{\mathrm{diff}} = 1$ kHz. The vibration amplitude of the sample was 0.32 nm. The full experimental details are described in Appx. 5.E.

To compare the different analytical (and numerical) solutions with the experimentally measured curve, we plotted the latter in red also in the background of Fig. 5.3B, 5.3C, and 5.3D. Figure 5.3B shows the solution for "standard nonlinear mixing". The discontinuities, in both the amplitude and the deflection, are due to the specific choice of tip-sample interaction (see Appx. 5.D). We observe that "standard nonlinear mixing" does not fit the measurement qualitatively. This is in contradiction with the general conception that standard nonlinear frequency mixing generates the observed signal in Heterodyne Force

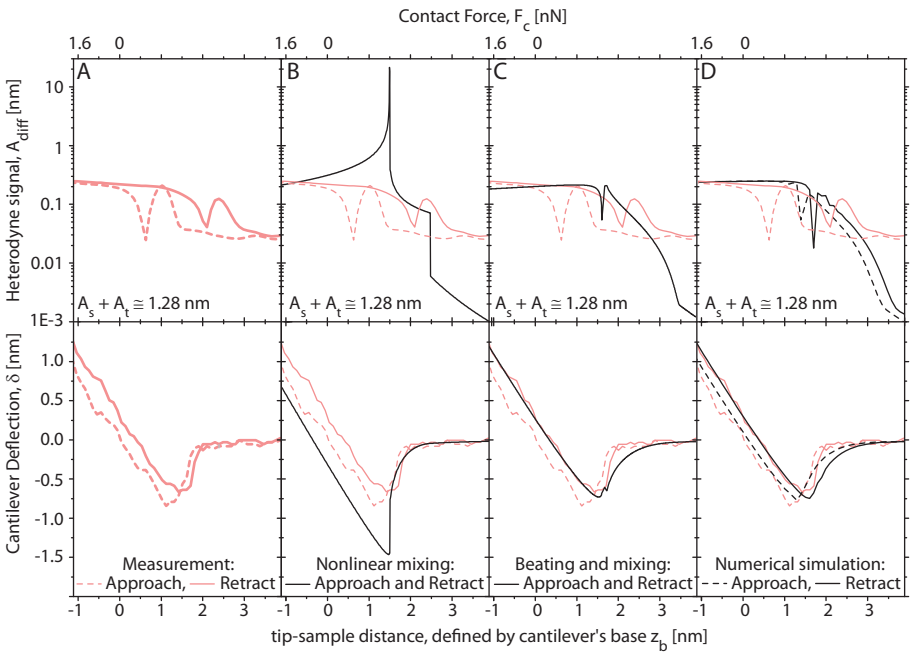


Figure 5.3: The heterodyne amplitude $A_{\text{diff}}$ as obtained from the experiment (A: red), from "standard nonlinear mixing" (B: black), from "beating and mixing" (C: black), and from a full numerical simulation (D: black). For comparison, the experimental curves (red) are also shown in the background of (B), (C), and (D). The bottom panels show the corresponding static deflection $\delta$ of the cantilever in the different methods. Notice that both the experimental results and the numerical calculations support the validity of "beating and mixing", as their curves qualitatively fit the "beating and mixing" ones. "Standard nonlinear mixing" deviates significantly.

Microscopy. In contrast, "beating and mixing", shown in Fig. 5.3C, does qualitatively fit the measured curve. The curvature is correctly reproduced at all tip-sample distances $z_b$. This confirms experimentally that "beating and mixing" generates the difference signal in Heterodyne Force Microscopy. Additional proof comes from a full numerical simulation (see Chap. 4 and [52]) that is shown in Fig. 5.3D. Again, the hysteresis is due to a lock-in. The full numerical simulation further supports "beating and mixing", as it qualitatively fits both the experimentally measured curves and the analytical "beating and mixing" solution.

Finally, let us discuss the general case of heterodyne measurements without a feedback to the input of the mixer as in Heterodyne Force Microscopy. We argue that even without feedback, beating is essential to correctly describe

the heterodyne detection. As the feedback term in a HFM is contained in $I_1$ (see Appx. 5.A.3), we can set $I_1$ to zero in Eq. 5.2. Note that the inverse transfer function $H^{-1}(\omega_{\text{diff}})$ is still necessary to correctly describe the force on the cantilever at the difference frequency. Also without feedback, "beating and mixing" still determines the heterodyne signal and the static deflection through the parameters $I_0$ and $I_2$. Therefore, we generally conclude that beating is of crucial importance for heterodyne detection schemes.

# Appendices of Chapter 5

## Materials and Methods

In the supplementary materials we discuss both the analytical methods and the experimental details that are needed to understand the dynamics in Heterodyne Force Microscopy, which is a nonlinear mechanical system driven simultaneously at two different frequencies.

In Appx. 5.A we derive analytical equations for the difference frequency generation considering only standard nonlinear mixing in Appx. 5.A.1, and a combination of beating and mixing in Appx. 5.A.2. Both solutions show that a nonlinear tip-sample interaction is required to produce a signal at the difference frequency. We show in Appx. 5.A.2 that both solutions are equal as long as the tip-sample interaction is purely quadratic. However, the solutions differ significantly, if the interaction is more nonlinear than purely quadratic, which is the case in Heterodyne Force Microscopy. The standard solution of mixing fails and, instead, one has to consider a combination of beating and mixing. The main essence is that the high frequency beating motion leads to two correction terms that alter the standard solution.

In a HFM the nonlinear tip-sample interaction generates a force at the difference frequency, which leads to a feedback on the tip-sample distance, as the cantilever really vibrates at the difference frequency. As a feedback mechanism is usually absent in standard nonlinear mixing, we discuss the solutions without feedback in Appx. 5.A.3 and obtain that beating still produces a correction term to the amplitude and the phase of the difference frequency in comparison to the standard solutions.

To evaluate the analytical solutions as a function of the tip-sample distance such that we can compare them with the difference frequency generation results from experiments, we need the inverse transfer function of the cantilever at the difference frequency, an expression for the tip-sample interaction, and the amplitudes $A_s$ and $A_t$ of the ultrasonic excitations of the sample and the cantilever respectively.

In Appx. 5.B we derive an analytical equation for the inverse transfer

function of the cantilever by making a mode expansion. To enable a correct comparison, we use values in the final description that match our experimental values as close as possible. In Appx. 5.D we fit an experimentally measured tip-sample interaction to obtain a realistic, analytical expression for it. Finally, we describe our experimental details in Appx.5.E, in which we also explain how we determine the amplitudes $A_s$ and $A_t$ of the ultrasonic excitations.

# 5.A Analytical Derivation of the Difference Frequency Generation

## 5.A.1 Difference Frequency Generation Considering Nonlinear Mixing only

In this appendix we provide the equations for standard nonlinear mixing as they are derived normally using a *second* order Taylor expansion. We start with an equation for the tip-sample distance $z$. This distance has a static offset $z_b$, which is given by the height of the base of the cantilever. In addition, we have to take into account a possible bending of the cantilever, which results in a change of $z$ and is described by the deflection $\delta$. Furthermore, the tip-sample distance $z$ contains the ultrasonic motion of both the cantilever at frequency $\omega_t$ and the sample at frequency $\omega_s$. Finally, we have to add a feedback term that accounts for a variation of $z$ at the difference frequency $\omega_{\text{diff}} = |\omega_s - \omega_t|$, as the cantilever really vibrates at $\omega_{\text{diff}}$ due to the effect of the nonlinear tip-sample interaction. If $H(\omega_{\text{diff}})$ denotes the transfer function of the cantilever that transfers a given force into an amplitude, the feedback term is given by $H(\omega_{\text{diff}})F(\omega_{\text{diff}})$, in which $F(\omega_{\text{diff}})$ describes the drive force on the cantilever at the difference frequency $\omega_{\text{diff}}$. To keep our description as general as possible, we do not make any assumptions on the drive force $F(\omega_{\text{diff}})$, and we evaluate $F(\omega_{\text{diff}})$ from the motion of the cantilever at the difference frequency such that $F(\omega_{\text{diff}}) = A_{\text{diff}}|H^{-1}(\omega_{\text{diff}})|\cos(\omega_{\text{diff}}t + \phi_{\text{diff}} + \Lambda)$, in which $|H^{-1}(\omega_{\text{diff}})|$ denotes the absolute value of the inverse transfer function of the cantilever and $\Lambda$ denotes the corresponding phase shift. Therefore, the feedback term is simply given by $A_{\text{diff}}\cos(\omega_{\text{diff}}t + \phi_{\text{diff}})$. This leads to the following equation for the tip-sample distance:

$$z = z_b + \delta + A_{\text{diff}}\cos(\omega_{\text{diff}}t + \phi_{\text{diff}}) + A_s\cos(\omega_s t + \phi_s) + A_t\cos(\omega_t t + \phi_t) \quad (5.4)$$

We use the derived expression for the tip-sample distance, Eq. 5.4, in the tip-sample interaction $F_{ts}(z)$ to find the effective drive force on the cantilever at the difference frequency. To take into account nonlinear mixing, we approximate the tip-sample interaction $F_{ts}(z)$ by a conventional *second* order Taylor expansion. Higher order terms are usually neglected, as their values are sufficiently small. The *square term* will produce a nonlinear mixing term. Since

we use a *second* order Taylor expansion that we evaluate in a *fixed, single point*, it is to be expected that the description holds exactly only for quadratic interactions.

$$\begin{aligned}
&F_{ts}\left(z_b+\delta+A_{\text{diff}}\cos(\omega_{\text{diff}}t+\phi_{\text{diff}})+\right.\\
&\qquad\left.A_s\cos(\omega_s t+\phi_s)+A_t\cos(\omega_t t+\phi_t)\right)=\\
&\quad F_{ts}(z_b+\delta)\\
&+\frac{\partial F_{ts}}{\partial z}(z_b+\delta)\left[A_{\text{diff}}\cos(\omega_{\text{diff}}t+\phi_{\text{diff}})+\right.\\
&\qquad\left.A_s\cos(\omega_s t+\phi_s)+A_t\cos(\omega_t t+\phi_t)\right]\\
&+\frac{1}{2}\frac{\partial^2 F_{ts}}{\partial z^2}(z_b+\delta)\left[A_{\text{diff}}\cos(\omega_{\text{diff}}t+\phi_{\text{diff}})+\right.\\
&\qquad\left.A_s\cos(\omega_s t+\phi_s)+A_t\cos(\omega_t t+\phi_t)\right]^2
\end{aligned}\tag{5.5}$$

As the high frequency motion of the cantilever is unaltered, see Chaps. 3 and 4 as well as [42, 52], and as we are only interested in the static deflection of the cantilever and its motion at the difference frequency $\omega_{\text{diff}}$, we evaluate Eq. 5.5 further and collect only the terms at zero frequency and the difference frequency $\omega_{\text{diff}}$. For the evaluation of the *square* term, we make use of

$$\cos(x)\cos(y)=0.5[\cos(x-y)+\cos(x+y)]\tag{5.6}$$

such that e.g.

$$[A_{\text{diff}}\cos(\omega_{\text{diff}}t+\phi_{\text{diff}})]^2=0.5A_{\text{diff}}^2+0.5A_{\text{diff}}^2\cos(2\omega_{\text{diff}}t+\phi_{\text{diff}})\tag{5.7}$$

and

$$\begin{aligned}
2A_sA_t\cos(\omega_s t+\phi_s)\cos(\omega_t t+\phi_t)=&A_sA_t\cos(\omega_{\text{diff}}t+[\phi_s-\phi_t])\\
&+A_sA_t\cos([\omega_s+\omega_t]t+[\phi_s+\phi_t]).
\end{aligned}\tag{5.8}$$

Keeping only the terms at zero frequency and at frequency $\omega_{\text{diff}}$, we find the following equation of motion

$$\begin{aligned}
&F_{ts}(z_b+\delta)\\
&+\frac{\partial F_{ts}}{\partial z}(z_b+\delta)\,A_{\text{diff}}\cos(\omega_{\text{diff}}t+\phi_{\text{diff}})\\
&+\frac{1}{2}\frac{\partial^2 F_{ts}}{\partial z^2}(z_b+\delta)\left[\frac{1}{2}A_{\text{diff}}^2+\frac{1}{2}A_s^2+\frac{1}{2}A_t^2+\underbrace{A_sA_t\cos(\omega_{\text{diff}}t+[\phi_s-\phi_t])}_{nonlinear\,mixing}\right]\\
&=k\delta+A_{\text{diff}}|H^{-1}(\omega_{\text{diff}})|\cos(\omega_{\text{diff}}t+\phi_{\text{diff}}+\Lambda)
\end{aligned}\tag{5.9}$$

, where k denotes the spring constant of the cantilever. The inverse transfer function $|H^{-1}(\omega_{\text{diff}})|$ is necessary to account for the force on the cantilever at the difference frequency $\omega_{\text{diff}}$. Both the inverse transfer function $H^{-1}(\omega_{\text{diff}})$ and the phase $\Lambda$ are defined below in Appx. 5.B. To derive a solution for the static deflection $\delta$ as well as for the amplitude $A_{\text{diff}}$ and the phase $\phi_{\text{diff}}$ of the difference frequency, we separate in Eq. 5.9 the static terms at zero frequency from those at the difference frequency $\omega_{\text{diff}}$. This results in the following two equations.

$$k\delta = F_{ts}(z_b+\delta) + \frac{1}{4}\frac{\partial^2 F_{ts}}{\partial z^2}(z_b+\delta)\left[A_{\text{diff}}^2 + A_s^2 + A_t^2\right] \tag{5.10}$$

$$\begin{aligned}\frac{\partial F_{ts}}{\partial z}(z_b+\delta)A_{\text{diff}}\cos(\omega_{\text{diff}}t+\phi_{\text{diff}}) + \\ \frac{1}{2}\frac{\partial^2 F_{ts}}{\partial z^2}(z_b+\delta)\,A_sA_t\cos(\omega_{\text{diff}}t+[\phi_s-\phi_t]) \\ = A_{\text{diff}}|H^{-1}(\omega_{\text{diff}})|\cos(\omega_{\text{diff}}t+\phi_{\text{diff}}+\Lambda)\end{aligned} \tag{5.11}$$

By using $\cos(A+B) = \cos(A)\cos(-B) + \sin(A)\sin(-B)$, Eq. 5.11 can be further evaluated to find a solution for $A_{\text{diff}}$ and $\phi_{\text{diff}}$

$$\begin{aligned}&\text{Re}\left[\frac{\partial F_{ts}}{\partial z}(z_b+\delta)\,A_{\text{diff}}e^{(\text{i}\omega_{\text{diff}}t+\text{i}\phi_{\text{diff}})}\right] + \\ &\qquad\text{Re}\left[\frac{1}{2}\frac{\partial^2 F_{ts}}{\partial z^2}(z_b+\delta)\,A_sA_te^{(\text{i}\omega_{\text{diff}}t+\text{i}\phi_{\text{diff}})}\right] \\ &= \text{Re}\left[A_{\text{diff}}|H^{-1}(\omega_{\text{diff}})|e^{(\text{i}\omega_{\text{diff}}t+\text{i}\phi_{\text{diff}}+\text{i}\Lambda)}\right]\end{aligned} \tag{5.12}$$

$$\begin{aligned}&\left[\frac{\partial F_{ts}}{\partial z}(z_b+\delta)\,A_{\text{diff}}e^{(\text{i}\phi_{\text{diff}})} + \frac{1}{2}\frac{\partial^2 F_{ts}}{\partial z^2}(z_b+\delta)\,A_sA_te^{(\text{i}\phi_{\text{diff}})}\right]e^{\text{i}\omega_{\text{diff}}t} \\ &= \left[A_{\text{diff}}|H^{-1}(\omega_{\text{diff}})|e^{(\text{i}\phi_{\text{diff}}+\text{i}\Lambda)}\right]e^{\text{i}\omega_{\text{diff}}t}\end{aligned} \tag{5.13}$$

This leads to the following two equations for the static deflection of the cantilever and the amplitude and the phase of the motion at the difference frequency:

$$\boxed{k\delta = F_{ts}(z_b+\delta) + \frac{1}{4}\frac{\partial^2 F_{ts}}{\partial z^2}(z_b+\delta)\left[A_{\text{diff}}^2 + A_s^2 + A_t^2\right]} \tag{5.14}$$

$$\boxed{A_{\text{diff}}e^{\text{i}\phi_{\text{diff}}} = \frac{\frac{1}{2}A_sA_t\frac{\partial^2 F_{ts}}{\partial z^2}(z_b+\delta)\,e^{\text{i}(\phi_s-\phi_t)}}{|H^{-1}(\omega_{\text{diff}})|e^{\text{i}\Lambda} - \frac{\partial F_{ts}}{\partial z}(z_b+\delta)}} \tag{5.15}$$

To enable a later comparison, we define $\hat{I_1} \equiv \frac{\partial F_{ts}}{\partial z}(z_b + \delta)$ and $\hat{I_2} \equiv \sqrt{A_s^2 + A_t^2}\frac{1}{2}\frac{\partial^2 F_{ts}}{\partial z^2}(z_b + \delta)$, such that

$$A_{\mathrm{diff}} e^{\mathrm{i}\phi_{\mathrm{diff}}} = \frac{\frac{A_s A_t}{\sqrt{A_s^2 + A_t^2}} \hat{I_2} e^{\mathrm{i}(\phi_s - \phi_t)}}{|H^{-1}(\omega_{\mathrm{diff}})| e^{\mathrm{i}\Lambda} - \hat{I_1}} \tag{5.16}$$

In Sect. 5.3, we compare the solution of Eqs. 5.14 and 5.15 with the experimental data and conclude that nonlinear mixing alone cannot explain the experimentally measured curves. To solve Eqs. 5.14 and 5.15 we need the inverse transfer function of the cantilever $H^{-1}(\omega_{\mathrm{diff}})$ (see Appx. 5.B), the tip-sample interaction $F_{ts}(z)$ (see Appx. 5.D), and the amplitudes $A_t$ and $A_s$ of the ultrasonic vibrations (see Appx. 5.E).

### 5.A.2 Difference Frequency Generation Considering Beating and Mixing

In the following we derive analytic expressions for the static deflection of the cantilever and its motion at the difference frequency by considering both beating and nonlinear mixing. We start with rewriting the ultrasonic, high frequency motions of the sample and the cantilever such that beating becomes evident.

$$\begin{aligned}
&A_s \cos(\omega_s t + \phi_s) + A_t \cos(\omega_t t + \phi_t) \\
&= \sqrt{A_t^2 + A_s^2 + 2A_s A_t \cos([\omega_s - \omega_t]\, t + [\phi_s - \phi_t])} \\
&\quad \times \cos\left(\frac{\omega_s + \omega_t}{2} t + \frac{\phi_s + \phi_t}{2} + \arctan\left[\frac{A_s - A_t}{A_s + A_t} \tan\left\{\frac{\omega_s - \omega_t}{2} t + \frac{\phi_s - \phi_t}{2}\right\}\right]\right) \\
&= \sqrt{A_t^2 + A_s^2 + 2A_s A_t \cos([\omega_s - \omega_t]\, t + [\phi_s - \phi_t])} \cdot \cos(\omega_h t + \phi_h)
\end{aligned} \tag{5.17}$$

, in which $\omega_h$ describes a high frequency motion with $\mathrm{Min}\{\omega_s, \omega_t\} < \omega_h < \mathrm{Max}\{\omega_s, \omega_t\}$ and $\phi_h$ denotes the phase corresponding to $\omega_h$. It is allowed to express the ultrasonic, high frequency motion with $\omega_h$ in Eq. 5.17, as is explained in the following. Firstly, the tangent of an angle oscillating at a single frequency $(\omega_s - \omega_t)/2$ is taken. Secondly, the tangent is multiplied with $(A_s - A_t)/(A_s + A_t)$, which alters the amplitude, but not the frequency. Thirdly, the amplitude is converted back to an angle, which still oscillates at a single frequency $(\omega_s - \omega_t)/2$. The argument of the cosine describing the high frequency motion is the sum of two angles: one oscillating at the sum frequency and one oscillating at the difference frequency. The net

result is a motion at a single, high frequency $\omega_h$.

Equation 5.17 shows that the variation of the tip-sample distance at the high, ultrasonic frequency $\omega_h$ has an amplitude modulation at frequency $\omega_{\text{diff}}$. We approximate the amplitude modulation by making only a *linear* expansion of Eq. 5.17, in which we make use of $\sqrt{1+2x} \approx 1+x; \forall x \ll 1$ with $x = A_s A_t/(A_s^2 + A_t^2)$. We find two terms that together describe the effective high frequency variation of the tip-sample distance.

$$\begin{aligned} & A_s \cos(\omega_s t + \phi_s) + A_t cos(\omega_t t + \phi_t) \qquad (5.18) \\ & = \underbrace{\sqrt{A_t^2 + A_s^2}\cos(\omega_h t + \phi_h)}_{z_{high}} + \underbrace{\frac{A_t A_s}{\sqrt{A_t^2 + A_s^2}} \underbrace{\cos(\omega_{\text{diff}} t + [\phi_s - \phi_t])}_{modulation} \underbrace{\cos(\omega_h t + \phi_h)}_{carrier\,frequency}}_{amplitude\,modulated\,z_{high}} \end{aligned}$$

Equation 5.18 consists of two terms, which are given by $z_{high}$ and an amplitude modulated term of $z_{high}$. The amplitude modulation is at the difference frequency such that the tip-sample distance is modulated in beats at $\omega_{\text{diff}}$. Beating does not excite new frequencies in a linear system. Although we are considering only beating with Eq. 5.18, the nonlinear tip-sample interaction *does* lead to a real excitation of the cantilever at the difference frequency. Keeping this in mind, we can write down the equation of motion for the cantilever, in which we include, in analogy to Appx. 5.A.1, a feedback term that explicitly describes the motion of the cantilever at the difference frequency.

$$\begin{aligned} & F_{ts}\left( z_b + \delta + A_{\text{diff}} \cos(\omega_{\text{diff}} t + \phi_{\text{diff}}) \right. \\ & \left. + \underbrace{\sqrt{A_t^2 + A_s^2}\cos(\omega_h t + \phi_h) + A_{\text{diff}}^{max} \cos(\omega_{\text{diff}} t + [\phi_s - \phi_t]) \cos(\omega_h t + \phi_h)}_{beating} \right) \\ & = k\delta + |H^{-1}(\omega_{\text{diff}})| A_{\text{diff}} \cos(\omega_{\text{diff}} t + \phi_{\text{diff}} + \Lambda) \qquad (5.19) \end{aligned}$$

, in which we keep the same definitions as in Appx. 5.A.1 and define $A_{\text{diff}}^{max}$ as

$$A_{\text{diff}}^{max} \equiv \frac{A_t A_s}{\sqrt{A_t^2 + A_s^2}} \qquad (5.20)$$

To find a solution to Eq. 5.19, we make, in analogy to Appx. 5.A.1, an expansion of the tip-sample force. This time, however, we only make a *linear*, first order Taylor expansion around a *time varying equilibrium position* of the cantilever to restrict ourself to the description of beating only and not to introduce a nonlinear term explicitly. This derivation is valid for all types of interactions including linear, quadratic, and all higher order of nonlinear dependencies.

$$
\begin{aligned}
&F_{ts}\Big(z_b+\delta+\sqrt{A_t^2+A_s^2}\cos(\omega_h t+\phi_h)\Big)\\
&+\left.\frac{\partial F_{ts}}{\partial z'}\right|_{z_b+\delta+\sqrt{A_t^2+A_s^2}\cos(\omega_h t+\phi_h)} A_{\mathrm{diff}}\cos(\omega_{\mathrm{diff}}t+\phi_{\mathrm{diff}})\\
&+\left.\frac{\partial F_{ts}}{\partial z'}\right|_{z_b+\delta+\sqrt{A_t^2+A_s^2}\cos(\omega_h t+\phi_h)} \frac{A_tA_s}{\sqrt{A_t^2+A_s^2}}\cos(\omega_{\mathrm{diff}}t+[\phi_s-\phi_t])\cos(\omega_h t+\phi_h)\\
&=k\delta+|H^{-1}(\omega_{\mathrm{diff}})|A_{\mathrm{diff}}\cos(\omega_{\mathrm{diff}}t+\phi_{\mathrm{diff}}+\Lambda) \qquad (5.21)
\end{aligned}
$$

, where, in analogy to Appx. 5.A.1, $|H^{-1}(\omega_{\mathrm{diff}})|$ is the inverse transfer function of the cantilever at the difference frequency $\omega_{\mathrm{diff}}$, and $\Lambda$ the corresponding frequency shift. Both the inverse transfer function $H^{-1}(\omega_{\mathrm{diff}})$ and the phase $\Lambda$ are defined below in Appx. 5.B.

In analogy to Eq. 5.9, we find the solutions for $A_{\mathrm{diff}}$, $\phi_{\mathrm{diff}}$, and the deflection $\delta$ of the cantilever by separating the terms of zero frequency and the terms at the difference frequency. However, as the arguments in Eq. 5.21 still contain an explicit time dependence, due to the high frequency motion of the cantilever, we first have to integrate over one period to find the solutions. For the zero frequency motion, e.g., one finds

$$\frac{1}{T}\int_0^T F_{ts}(z_b+\delta+\sqrt{A_s^2+A_t^2}\cos(\omega_h t+\phi_h))dt=\frac{1}{T}\int_0^T k\delta dt=k\delta \qquad (5.22)$$

This leads to the following two expressions

$$\boxed{k\delta=I_0} \qquad (5.23)$$

$$\boxed{A_{\mathrm{diff}}e^{i\phi_{\mathrm{diff}}}=\frac{A_{\mathrm{diff}}^{max}I_2e^{\mathrm{i}(\phi_s-\phi_t)}}{|H^{-1}(\omega_{\mathrm{diff}})|e^{\mathrm{i}\Lambda}-I_1}} \qquad (5.24)$$

in which $I_0$, $I_1$, and $I_2$ are integrals characterizing the tip-sample interaction.

$$
\begin{aligned}
I_0&=\frac{1}{T}\int_0^T F_{ts}\left(z_b+\delta+\sqrt{A_t^2+A_s^2}\cos(\omega_h t+\phi_h)\right)dt\\
&=\frac{1}{\pi}\int_{-1}^1 F_{ts}\left(z_b+\delta+\sqrt{A_t^2+A_s^2}u\right)\frac{du}{\sqrt{1-u^2}} \qquad (5.25)\\
I_1&=\frac{1}{T}\int_0^T \frac{\partial F_{ts}}{\partial z}\left(z_b+\delta+\sqrt{A_t^2+A_s^2}\cos(\omega_h t+\phi_h)\right)dt\\
&=\frac{1}{\pi}\int_{-1}^1 \frac{\partial F_{ts}}{\partial z'}\left(z_b+\delta+\sqrt{A_t^2+A_s^2}u\right)\frac{du}{\sqrt{1-u^2}} \qquad (5.26)\\
I_2&=\frac{1}{T}\int_0^T \frac{\partial F_{ts}}{\partial z}\left(z_b+\delta+\sqrt{A_t^2+A_s^2}\cos(\omega_h t+\phi_h)\right)\cos(\omega_{high}t)dt\\
&=\frac{1}{\pi}\int_{-1}^1 \frac{\partial F_{ts}}{\partial z'}\left(z_b+\delta+\sqrt{A_t^2+A_s^2}u\right)\frac{udu}{\sqrt{1-u^2}} \qquad (5.27)
\end{aligned}
$$

The integrals over the parameter $u$ (right hand side) in equations 5.25 ,5.26, and 5.27 are obtained by using an Abel transform of the integrals over time $T = 2\pi/\omega_h$. As we integrate over one period $T$, the integrals become independent of $\phi_h$ and we can set the phase $\phi_h$ to 0.

Equation 5.24 shows that $|A_{\mathrm{diff}}|$ depends on both integrals $I_1$ and $I_2$. The integral $I_1$ represents an effective (average) spring constant describing the tip-sample stiffness, as $I_1$ integrates $\partial F_{ts}/\partial z$ over one period of the high frequency motion of the cantilever. The other integral $I_2$, describes the difference frequency generation via a combination of beating and nonlinear mixing. This becomes evident, if we partially integrate Eq. 5.27:

$$\begin{aligned} I_2 &= \frac{1}{\pi}\int_{-1}^{1} \frac{\partial F_{ts}}{\partial z'}\left(z_b + \delta + \sqrt{A_t^2 + A_s^2}u\right)\frac{udu}{\sqrt{1-u^2}} \\ &= \frac{\sqrt{A_t^2 + A_s^2}}{2\pi}\int_{-1}^{1} \frac{\partial^2 F_{ts}}{\partial z'^2}\left(z_b + \delta + \sqrt{A_t^2 + A_s^2}u\right)\sqrt{1-u^2}du \end{aligned} \tag{5.28}$$

A linear tip-sample interaction implies that $\partial F_{ts}/\partial z$ is constant and $\partial^2 F_{ts}/\partial z^2 = 0$, which results in $I_2 = 0$. As a consequence, there is no difference frequency generation ($A_{\mathrm{diff}} = 0$). This is in perfect agreement with the derivation of $A_{\mathrm{diff}}$ considering only nonlinear mixing (Eq. 5.15): $A_{\mathrm{diff}} = 0$, if $\partial^2 F_{ts}/\partial z^2 = 0$. We conclude that both derivations require a nonlinear tip-sample interaction to generate a signal at the difference frequency. Please note that, although starting the description with pure beating and using only linear expansions, nonlinear mixing is not excluded for the solutions provided in Eqs. 5.23 and 5.24, as we did not include any restrictions on the particular tip-sample interaction: the equations hold also for a nonlinear tip-sample interaction.

It is instructive to see that Eq. 5.24 becomes equal to Eq. 5.16 for the special case of a *quadratic* tip-sample interaction, in which $\partial F_{ts}/\partial z$ is linear and $\partial^2 F_{ts}/\partial z^2$ is constant.

$$\begin{aligned} I_1 &= \frac{1}{\pi}\int_{-1}^{1} \frac{\partial F_{ts}}{\partial z}(z_b + \delta + \sqrt{A_s^2 + A_t^2}u)\frac{du}{\sqrt{1-u^2}} \\ &= \frac{\partial F_{ts}}{\partial z}(z_b + \delta) \end{aligned} \tag{5.29}$$

$$\begin{aligned} I_2 &= \frac{\sqrt{A_s^2 + A_t^2}}{2\pi}\int_{-1}^{1} \frac{\partial^2 F_{ts}}{\partial z^2}(z_b + \delta + \sqrt{A_s^2 + A_t^2}u)\sqrt{1-u^2}du \\ &= \frac{\sqrt{A_s^2 + A_t^2}}{2}\frac{\partial^2 F_{ts}}{\partial z^2}(z_b + \delta) \end{aligned} \tag{5.30}$$

One sees that, in this special case, $I_1 = \hat{I}_1$ and $I_2 = \hat{I}_2$. The "standard" solution of nonlinear mixing (Eq. 5.16) delivers the "correct" solution as long as the

interaction is only quadratic. For Heterodyne Force Microscopy, the tip-sample interaction deviates significantly from a quadratic behavior and Eqs. 5.23 and 5.24 are needed to correctly describe the solutions: a combination of beating and mixing takes place in this case. The high frequency beating components lead to two correction terms. $I_1$ describes the average of $\partial F_{ts}/\partial z$ for the high frequency beating component, whereas $I_2$ describes the weighted average of $\partial F_{ts}/\partial z$, where the weighing is done by the cosine term. A proper description of nonlinear mixing requires, therefore, that one also takes into account the high frequency beating motion for all interactions that deviate from that of a pure quadratic form.

For the sake of completeness, we evaluate Eq. 5.19 in the following also to *second* order

$$
\begin{aligned}
&F_{ts}\Big(z_b+\delta+\sqrt{A_t^2+A_s^2}\cos(\omega_h t+\phi_h)\Big)\\
&+\left.\frac{\partial F_{ts}}{\partial z'}\right|_{z_b+\delta+\sqrt{A_t^2+A_s^2}\cos(\omega_h t+\phi_h)} A_{\mathrm{diff}}\cos(\omega_{\mathrm{diff}}t+\phi_{\mathrm{diff}})\\
&+\left.\frac{\partial F_{ts}}{\partial z'}\right|_{z_b+\delta+\sqrt{A_t^2+A_s^2}\cos(\omega_h t+\phi_h)} \frac{A_tA_s}{\sqrt{A_t^2+A_s^2}}\cos(\omega_{\mathrm{diff}}t+[\phi_s-\phi_t])\cos(\omega_h t+\phi_h)\\
&+\frac{1}{4}\left.\frac{\partial^2 F_{ts}}{\partial z'^2}\right|_{z_b+\delta+\sqrt{A_t^2+A_s^2}\cos(\omega_h t+\phi_h)} \times\\
&\qquad\left[\begin{array}{l}(A_{\mathrm{diff}}^{max})^2\cos^2(\omega_h t+\phi_h)\\ +2A_{\mathrm{diff}}A_{\mathrm{diff}}^{max}\cos\left([\phi_s-\phi_t]-\phi_{\mathrm{diff}}\right)\cos(\omega_h t+\phi_h)\\ +A_{\mathrm{diff}}^2\end{array}\right]\\
&=k\delta+|H^{-1}(\omega_{\mathrm{diff}})|A_{\mathrm{diff}}\cos(\omega_{\mathrm{diff}}t+\phi_{\mathrm{diff}}+\Lambda) \qquad (5.31)
\end{aligned}
$$

By separating the components with zero frequency and the difference frequency, we find the following solutions:

$$
\begin{aligned}
k\delta &= I_0+\tfrac{1}{4}I_3A_{\mathrm{diff}}^2+\\
&\quad \tfrac{1}{2}I_4A_{\mathrm{diff}}A_{\mathrm{diff}}^{max}\cos\left([\phi_s-\phi_t]-\phi_{\mathrm{diff}}\right)+\tfrac{1}{4}I_5\left(A_{\mathrm{diff}}^{max}\right)^2 \qquad (5.32)\\
A_{\mathrm{diff}}e^{\mathrm{i}\phi_{\mathrm{diff}}} &= \frac{A_{\mathrm{diff}}^{max}I_2e^{\mathrm{i}(\phi_s-\phi_t)}}{H^{-1}e^{\mathrm{i}\Lambda}-I_1} \qquad (5.33)
\end{aligned}
$$

, in which the terms $I_0$, $I_1$, and $I_2$ are given by Eqs. 5.25, 5.26, and 5.27, and

$$I_3 = \frac{1}{T}\int_0^T \frac{\partial^2 F_{ts}}{\partial z'^2}\left(z_b+\delta+\sqrt{A_t^2+A_s^2}\cos(\omega_h t+\phi_h)\right)dt$$
$$= \frac{1}{\pi}\int_{-1}^{1} \frac{\partial^2 F_{ts}}{\partial z'^2}\left(z_b+\delta+\sqrt{A_t^2+A_s^2}u\right)\frac{du}{\sqrt{1-u^2}} \tag{5.34}$$
$$I_4 = \frac{1}{T}\int_0^T \frac{\partial^2 F_{ts}}{\partial z'^2}\left(z_b+\delta+\sqrt{A_t^2+A_s^2}\cos(\omega_h t+\phi_h)\right)\cos(\omega_h t+\phi_h)dt$$
$$= \frac{1}{\pi}\int_{-1}^{1} \frac{\partial^2 F_{ts}}{\partial z'^2}\left(z_b+\delta+\sqrt{A_t^2+A_s^2}u\right)\frac{udu}{\sqrt{1-u^2}} \tag{5.35}$$
$$I_5 = \frac{1}{T}\int_0^T \frac{\partial^2 F_{ts}}{\partial z'^2}\left(z_b+\delta+\sqrt{A_t^2+A_s^2}\cos(\omega_h t+\phi_h)\right)\cos^2(\omega_h t+\phi_h)dt$$
$$= \frac{1}{\pi}\int_{-1}^{1} \frac{\partial^2 F_{ts}}{\partial z'^2}\left(z_b+\delta+\sqrt{A_t^2+A_s^2}u\right)\frac{u^2du}{\sqrt{1-u^2}} \tag{5.36}$$

Even if we evaluate Eq. 5.19 with a nonlinear second order expansion, we find the same solution for $A_{\text{diff}}$ and $\phi_{\text{diff}}$ (compare Eq. 5.24 with Eq. 5.33). The nonlinear second order expansion delivers only correction terms for the deflection $\delta$, see $I_3$, $I_4$, and $I_5$ in Eq. 5.32.

### 5.A.3 Difference Frequency Generation without Feedback to the Input Signal

In appendices 5.A.1 and 5.A.2 we considered the difference frequency generation, in which we included a term that explicitly describes the motion of the cantilever at the difference frequency. This term acts as a feedback mechanism and has a back action on the result obtained for the amplitude $A_{\text{diff}}$ and the phase $\phi_{\text{diff}}$ of the difference frequency. In Heterodyne Force Microscopy this feedback is very important, but in other typical nonlinear systems this feedback is mostly absent. In this appendix we consider the results for the difference frequency generation *without* the back action on the input signals.

Let us first discuss the case where the difference frequency generation is caused by nonlinear mixing only. Without feedback, we remove the motion of the cantilever at the difference frequency from Eq. 5.5 and obtain an expression for the mixing by making a second order Taylor expansion of the tip-sample interaction:

$$F_{ts}\left(z_b+\delta+A_s\cos(\omega_s t+\phi_s)+A_t\cos(\omega_t t+\phi_t)\right) = \tag{5.37}$$
$$F_{ts}(z_b+\delta)$$
$$+\quad \frac{\partial F_{ts}}{\partial z}(z_b+\delta)\left[A_s\cos(\omega_s t+\phi_s)+A_t\cos(\omega_t t+\phi_t)\right]$$
$$+\frac{1}{2}\quad \frac{\partial^2 F_{ts}}{\partial z^2}(z_b+\delta)\left[A_s\cos(\omega_s t+\phi_s)+A_t\cos(\omega_t t+\phi_t)\right]^2$$

Using the same derivation as described in Appx. 5.A.1, we obtain an expression for the amplitude $A_{\text{diff}}$ and the phase $\phi_{\text{diff}}$ of the difference frequency:

$$A_{\text{diff}} e^{\mathrm{i}\phi_{\text{diff}}} = \frac{A_{\text{diff}}^{max} \hat{I}_2 e^{\mathrm{i}(\phi_s - \phi_t)}}{|H^{-1}(\omega_{\text{diff}})| e^{\mathrm{i}\Lambda}} \text{ , in which } \hat{I}_2 = \frac{\sqrt{A_s^2 + A_t^2}}{2} \frac{\partial^2 F_{ts}}{\partial z^2}(z_b + \delta) \tag{5.38}$$

Let us now consider the case where both beating and nonlinear mixing are important. By comparing Eqs. 5.16 and 5.38, we notice that we could have obtained Eq. 5.38 by setting $\hat{I}_1$ to zero in Eq. 5.16. A similar argument holds for the case where both beating and nonlinear mixing are considered. By setting $I_1$ to zero in Eq. 5.24, we obtain the following expression for the amplitude $A_{\text{diff}}$ and the phase $\phi_{\text{diff}}$ of the difference frequency:

$$\begin{aligned} A_{\text{diff}} e^{\mathrm{i}\phi_{\text{diff}}} &= \frac{A_{\text{diff}}^{max} I_2 e^{\mathrm{i}(\phi_s - \phi_t)}}{|H^{-1}(\omega_{\text{diff}})| e^{\mathrm{i}\Lambda}} \\ \text{, in which } I_2 &= \frac{\sqrt{A_s^2 + A_t^2}}{2\pi} \int_{-1}^{1} \frac{\partial^2 F_{ts}}{\partial z^2}(z_b + \delta + \sqrt{A_s^2 + A_t^2}u)\sqrt{1-u^2}du \end{aligned} \tag{5.39}$$

In conclusion, even without feedback, the solutions to $A_{\text{diff}}$ and $\phi_{\text{diff}}$ differ significantly between "standard nonlinear mixing" and "beating and mixing" (compare Eqs. 5.38 and 5.39). Described by $I_2$ in Eq. 5.39, a correction is required that explicitly accounts for the high frequency motion. The solutions to $A_{\text{diff}}$ and $\phi_{\text{diff}}$ become equal, if $\hat{I}_2$ is equal to $I_2$. This is only the case for a pure *quadratic* tip-sample interaction or nonlinearity.

## 5.B Transfer Function of the Cantilever at the Difference Frequency

In Appx. 5.A we derived analytical expressions for the amplitude and phase of the difference frequency generation. To solve these equations, we need the inverse transfer function $H^{-1}(\omega_{\text{diff}})$ of the cantilever at the difference frequency that transfers a given amplitude into a force, as well as its associated phase shift $\Lambda$. As the difference frequency $\omega_{\text{diff}}$ is smaller than the first resonance frequency of the cantilever $\omega_0$, we can use the expression of the phase and the amplitude of an harmonic oscillator for the transfer function $H^{-1}(\omega_{\text{diff}})$ and $\Lambda$ respectively:

$$\Lambda = \tan^{-1}\left[\frac{\omega_{\text{diff}}\omega_0/Q_0}{\omega_0^2 - \omega_{\text{diff}}^2}\right] \tag{5.40}$$

$$H^{-1}(\omega_{\text{diff}}) = \frac{1}{\phi_0(L)^2}\sqrt{(\omega_0^2 - \omega_{\text{diff}}^2)^2 + \left(\frac{\omega_0\omega_{\text{diff}}}{Q_0}\right)^2} \tag{5.41}$$

, in which $Q_0$ denotes the quality factor of the first resonance, $\phi_0(L)$ the mode shape at the end of the cantilever, and L the length of the cantilever.

To derive an expression for $\phi_0(L)$ and $\Lambda$, we calculate in the following the resonance frequencies, and thus the transfer function, of the cantilever in contact with the sample. If the cantilever approaches the surface, the changing tip-sample interaction leads to a change of the transfer function and a frequency shift of the first mode. To find the frequency shift associated with the tip-sample interaction, we employ the Euler-beam equation [32, 45, 49, 50].

$$\begin{aligned} EI\frac{\partial}{\partial x^4}\left[\Phi(x,t)+a_i\frac{\partial\Phi}{\partial t}\right]+\rho W h\frac{\partial\Phi}{\partial t^2} \\ +a_h\frac{\partial\Phi}{\partial t}-\delta(x-L)\left[F_{ts}(z)+F_{drive}(t)\right]=0 \end{aligned} \tag{5.42}$$

, in which $E$ is the Young's modulus of the cantilever, $I$ is the moment of inertia, $a_i$ is the internal damping coefficient, $\rho$ is the density, $W$, $h$, and $L$ are, respectively, the width, height, and length of the cantilever, $a_h$ is the hydrodynamic damping, and $\Phi(x,t)$ is the vertical displacement of the cantilever at position $x$ and at time $t$. $F_{drive}$ is the drive force on the cantilever at its free end and $F_{ts}(z)$ represents the tip-sample interaction acting on the free end, where $z$ is the tip-sample distance.

We calculate the frequency shift of the cantilever modes by recognizing that a change in boundary conditions applies, if a tip-sample interaction is present. In analogy to Rabe [45] we change the boundary conditions at the free end of the cantilever such that

$$\begin{aligned} \left[EI\frac{\partial^3\Phi(x,t)}{\partial x^3}-M_t\frac{\partial^2\Phi(x,t)}{\partial t^2}\right]_{x=L} &= -I_1\Phi(x,t) \qquad \Phi(0,t) &= 0 \\ \left[EI\frac{\partial^2\Phi(x,t)}{\partial x^2}+I_t\frac{\partial^3\Phi(x,t)}{\partial t^2\partial x}\right]_{x=L} &= 0 \qquad \left.\frac{\partial\Phi(x,t)}{\partial x}\right|_{x=0} &= 0 \end{aligned} \tag{5.43}$$

, in which $M_t$ denotes the mass of the tip, $I_t$ the moment of inertia of the tip, and $I_1$ an effective tip-sample spring given by Eq. 5.26. These boundary conditions introduce a discrete set of solutions such that it is possible to solve Eq. 5.42 by using the ansatz $\Phi(x,t)=\phi(x)\eta(t)$. The general solution of Eq. 5.42, obeying the boundary conditions at $x=0$, is

$$\phi(x)=A\left[\cos\left(\lambda\frac{x}{L}\right)-\cosh\left(\lambda\frac{x}{L}\right)\right]+C\left[\sin\left(\lambda\frac{x}{L}\right)-\sinh\left(\lambda\frac{x}{L}\right)\right] \tag{5.44}$$

, in which $A$ and $C$ are constants to be determined by the boundary conditions at $x=L$, and $\lambda$ is the wave number related to the frequency $\omega$ as

$$\omega^2=\left(\frac{\lambda}{L}\right)^4\frac{EI}{m} \tag{5.45}$$

, in which $m$ denotes the mass per unit length of the cantilever beam.

We solve the boundary conditions at $x = L$ as follows. Firstly, we observe that $-I_1\Phi(L,t)$ can be transferred to the left hand side of the first equation in Eq. 5.43.

$$\left[EI\frac{\partial^3\Phi(x,t)}{\partial x^3} - M_t\frac{\partial^2\Phi(x,t)}{\partial t^2} + I_1\Phi(x,t)\right]_{x=L} = 0 \tag{5.46}$$

Secondly, we substitute the second derivative to time of $\Phi(x,t)$, which equals $-\omega^2\Phi(x,t)$.

$$\left[EI\frac{\partial^3\Phi(x,t)}{\partial x^3} + M_t\omega^2\Phi(x,t)\left(1 + \frac{I_1}{M_t\omega^2}\right)\right]_{x=L} = 0 \tag{5.47}$$

Finally, we recognize that we obtain the solution as described in [51], but with a different effective tip mass: we have to substitute $M_t$ in their solution with

$$M_t \to M_t\left(1 + \frac{mI_1L^4}{EIM_t\lambda^4}\right) \tag{5.48}$$

The resonance frequencies are obtained from the characteristic equation in [51], in which we replace $M_t$ as given by Eq. 5.48. After a straightforward calculation, we find the following expression

$$\begin{aligned} &1 + \cos\lambda\cosh\lambda + \frac{M_t\lambda}{EI}\left[\cos\lambda\sinh\lambda - \sin\lambda\cosh\lambda\right] \\ &- \frac{I_t\lambda^3}{mL^3}\left[\cosh\lambda\sin\lambda + \sinh\lambda\cos\lambda\right] + \frac{M_tI_t\lambda^4}{m^2L^4}\left[1 - \cos\lambda\cosh\lambda\right] \\ &+ \frac{L^3I_1}{EI\lambda^3}\left[\cos\lambda\sinh\lambda - \sin\lambda\cosh\lambda\right] + \frac{I_tI_1}{EIm}\left[1 - \cos\lambda\cosh\lambda\right] = 0 \end{aligned} \tag{5.49}$$

The resonance frequencies of the cantilever are obtained from the discrete set of solutions of $\lambda$ to Eq. 5.49 and the dispersion relation of Eq. 5.45. Please note that Eq. 5.49 reduces to the result obtained by Rabe [45], if $M_t = 0$ and $I_t = 0$, i.e. no tip mass and no tip moment of inertia.

We derived the equations to determine the resonance frequencies of a cantilever with tip mass $M_t$ and tip moment of inertia $I_t$ moving in a general tip-sample interaction. The inverse transfer function necessary to calculate the excitation of the difference frequency needs the first resonance frequency. Equipped with the first resonance frequency $\omega_0$, we need $\phi_0(L)$ to finally calculate the inverse transfer function $H^{-1}(\omega_{\text{diff}})$ (see Eq. 5.41). We find the allowed modes from the discrete set of solutions of $\lambda$ to Eq. 5.49, which gives us $\lambda_r$ for mode $r$. Applying the substitution of Eq. 5.48 to the mass-normalized solutions found in [51], we find for $\phi_r(x)$

$$\phi_r(x) = A_r\left[\cos\lambda_r\frac{x}{L} - \cosh\lambda_r\frac{x}{L} + \xi_r\left(\sin\lambda_r\frac{x}{L} - \sinh\lambda_r\frac{x}{L}\right)\right] \tag{5.50}$$

, in which $\xi_r$ is given by

$$\xi_r = \frac{\sin\lambda_r - \sinh\lambda_r + \lambda_r\left(\frac{M_t}{mL} + \frac{I_1 L^3}{EI\lambda_r^4}\right)(\cos\lambda_r - \cosh\lambda_r)}{\cos\lambda_r + \cosh\lambda_r - \lambda_r\left(\frac{M_t}{mL} + \frac{I_1 L^3}{EI\lambda_r^4}\right)(\sin\lambda_r - \sinh\lambda_r)} \tag{5.51}$$

, and $A_r$ is determined from the normalization

$$\int_0^L \frac{\partial^2\phi_r(x)}{\partial x^2} EI \frac{\partial^2\phi_s(x)}{\partial x^2} dx = \omega_r^2 \delta_{rs} \tag{5.52}$$

, in which $\delta_{rs}$ is the Kronecker delta. Finally, we determine $\phi_0(L)$ from Eqs. 5.50, 5.51, and 5.52.

As it is important for the frequency shift sensitivity of the cantilever, please note that the effect of the tip-sample interaction on the mode shape is proportional to $I_1/\lambda_r(I_1)^4$ (see explicit dependence of the tip-sample interaction in equation (5.51)). In analogy to the cantilevers used in our experiments, we assumed a standard Silicon cantilever for our numerical calculations with a stiffness of 2 N/m and its first flexural mode at 73.4 kHz. The cantilever has a length of $L = 230\,\mu$m, a width of $W = 30\,\mu$m, a height of $h = 2.7\,\mu$m, a Young's modulus of $E = 179$ GPa, a density of $\rho = 2330$ kg/m$^3$, an internal damping of $a_i = 4.3 \cdot 10^{-10}$ s, a hydrodynamic damping of $a_h = 5.6 \cdot 10^{-4}$ kg m$^2$ s, a tip mass of $M_t = 5.4 \cdot 10^{-15}$ kg, and a moment of inertia of the tip of $I_t = 3 \cdot 10^{-22}$ kg m$^2$. The wave numbers $\lambda_r(I_1 = 0)$ for this cantilever without tip-sample interaction are given in Tab. 1. Also shown in Tab. 1 are the proportionality constants $1/\lambda_r^4(I_1 = 0)$, which determine the frequency shift sensitivity, $I_1/\lambda_r^4(I_1 = 0)$ see equation (5.49), of a mode to the tip-sample interaction [1]. We see that the $3^{rd}$ mode of the cantilever is three orders of

| r | $\lambda_r$ | $\omega_r/2\pi$ | $\lambda_r^{-4}$ |
|---|---|---|---|
| 0 | 1.87441 | 73.4 kHz | 8.1 $10^{-4}$ |
| 1 | 4.67949 | 456 kHz | 2.1 $10^{-5}$ |
| 2 | 7.78852 | 1.27 MHz | 2.7 $10^{-6}$ |
| 3 | 10.8007 | 2.44 MHz | 7.3 $10^{-7}$ |
| 4 | 13.6737 | 3.91 MHz | 2.9 $10^{-7}$ |

Table 5.2: The wave numbers $\lambda_r(I_1 = 0)$ for mode $r$, the resonance frequencies $\omega_r(I_1 = 0)/2\pi$, and the proportionality constants $\lambda_r^{-4}(I_1 = 0)$, which determine the frequency shift sensitivity, $I_1/\lambda_r^4(I_1 = 0)$ see equation (5.49), of a mode to the tip-sample interaction.

[1] For small contact forces, the following equation holds in first approximation: $\lambda_r(I_1) \approx \lambda_r(I_1 = 0)$.

magnitude less sensitive to the tip-sample interaction than the $0^{th}$ mode of the cantilever. This is why the ultrasonic vibration of the cantilever at, e.g., frequency $f_s = 2.8$ MHz is relatively insensitive to the tip-sample interaction.

## 5.C Resonance Frequency Shifts of the Canitlever Modes

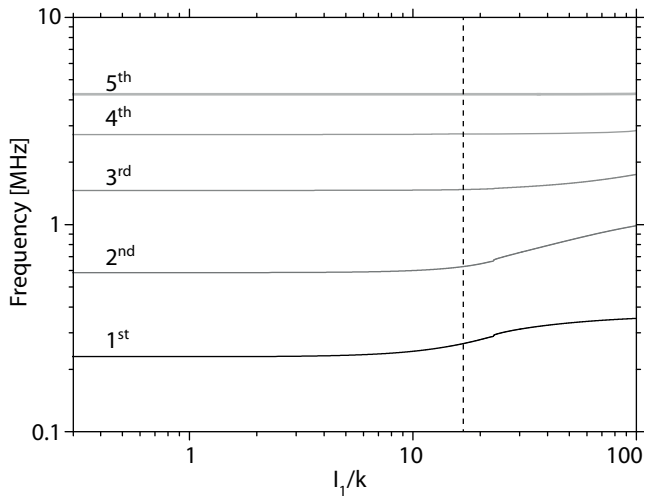


Figure 5.4: The resonance frequencies of the first 5 modes of the cantilever as a function of the normalized tip-sample contact $I_1/k$. $I_1$ is the effective tip-sample spring that has to be taken into account at the free end of the cantilever when getting into contact with the sample, and $k = 2$ N/m is the spring constant of the cantilever. The resonance frequency shifts reduce for the higher modes as these modes get stiffer with increasing resonance frequency. Strictly speaking, the contact resonances, which describe the situation with a node at the free end of the cantilever, are reached only for an infinitely stiff sample ($I_1$). The vertical dashed line indicates the maximum tip-sample stiffness that we reach in all experiments described in this thesis.

## 5.D Characterizing the Tip-Sample Interaction

For our numerical calculations, in appendices 5.A and 5.B, we need the tip-sample interaction or force $F_{ts}(z)$. In general, an accurate measurement of the tip-sample interaction using an atomic force microscope is difficult and is, at the present day, still an area of ongoing research [66]. In our experiments, which were performed in air, we used a cantilever, of which we calibrated the

spring constant $k$ to be $2.0 \pm 0.4$ N/m using the thermal noise method [67]. During the measurements, we recorded not only the amplitude at the difference frequency but simultaneously also the deflection $\delta$. We have to compare the tip-sample interaction $k \cdot \delta$, obtained from the measurements, with the average force $I_0$, obtained from our numerical calculations (see Eq. 5.23). This is an approximation, as we neglect the higher order contributions of $I_3$, $I_4$, and $I_5$ in Eq. 5.32. Anyhow, it provides us with a good estimate of the tip-sample interaction that we use in the numerical calculations.

Figure 5.5 shows the obtained force-distance curves, in which the experimentally measured curve is indicated in red, and the fit to it that is used in our analytical calculations, is indicated with a dashed black line. We fitted the experimental curve with a modified Derjaguin-Muller-Toporov (DMT-) model, see Sect. 1.4 and [23], in which we removed the discontinuity in the first derivative by inserting two parabolic functions. As a result we got the following analytical expression for the force-distance curve

$$F_{ts}(z) = \begin{cases} -\dfrac{HR}{6a_0^2} + \dfrac{4}{3}E_f\sqrt{R}(a_0 - z)^{3/2} & \text{if } z < -0.67\text{nm}, \\ \alpha_1 z^2 + \alpha_2 z + \alpha_3 & \text{if } -0.67\text{nm} \leq z \leq a_0, \\ \beta_1 z^2 + \beta_2 z + \beta_3 & \text{if } a_0 \leq z \leq 2.62\text{nm} \\ -\dfrac{HR}{6z^2} & \text{if } z > 3a_0. \end{cases} \tag{5.53}$$

, in which the radius $R$ of the cantilever's tip is 0.14 nm, the Hamaker constant $H$ is $30 \cdot 10^{-18}$ J, the distance $a_0$ is 0.25 nm, and $E_f$ is an effective Young's modulus describing the tip-sample stiffness equal to 61 GPa.

As can be seen from Eq. 5.53, we locally approximate $F_{ts}(z)$ with two quadratic functions: one for $-0.67\,\text{nm} \leq z \leq a_0$, and one for $a_0 \leq z \leq 2.62$ nm such that both $F_{ts}(z)$ and $\partial F_{ts}(z)/\partial z$ are continuous at $z = -0.67$ nm, $z = a_0$, and $z = 2.62$ nm. These constraints determine the parameters $\{\alpha_1, \alpha_2, \alpha_3\}$ and $\{\beta_1, \beta_2, \beta_3\}$. We used this procedure to obtain an analytical expression for the experimental tip-sample interaction and note that we do not have an absolute $z$-scale. Therefore, the parameters obtained for $F_{ts}(z)$ do not describe the material properties of Silicon.

We obtained the Young's modulus on Silicon by fitting an experimentally obtained tip-sample interaction $F_{ts}$ with the DMT-model. A parameter called $\lambda$, which is related to the elasticities of the tip and the sample, is usually used to differentiate between the applicabilities of different models that describe the tip-sample interaction, see Fig. 1.8 and [27]. As $\lambda = 0.85$ in our case, one should use the Maugis-Dugdale (M-D-) model [25]. Nevertheless, our approach with the DMT-model is fully justified, as we have demonstrated in Chap. 4 and in [52] that it does not matter at all for the numerical simulations which of the models describes the tip-sample interaction, as long as the fit perfectly

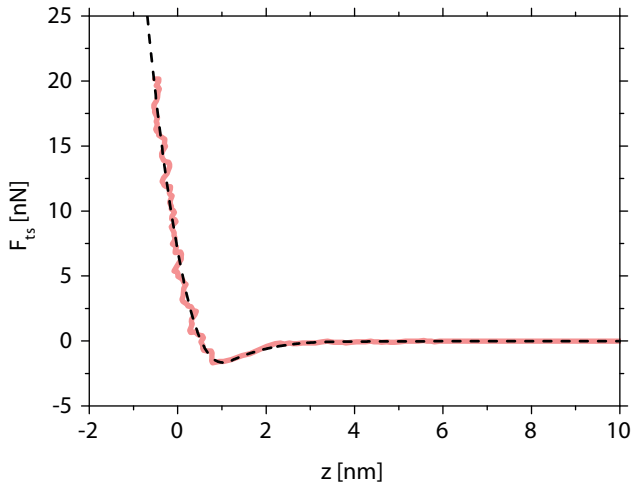


Figure 5.5: Force versus distance curves from measurements with a hard Silicon tip/cantilever pushing into a hard Silicon wafer: obtained from the experiment (red) and as used in the analytical calculation (dashed black). Please note that $F_{ts}(z = 0) \neq 0$ per definition.

matches the (experimentally obtained) tip-sample interaction. The only thing that matters is the particular shape (form) of $F_{ts}(z)$ and *not* the model that is used to describe this particular interaction. In addition, please note that it is almost impossible to use the M-D-model, as it does not provide an analytical expression for $F_{ts}$ such that it can only be solved iteratively, if the value of $\lambda$ is not known a priori.

Finally we would like to mention that the obtained tip-sample stiffness of 61 GPa fits very well with the Young's modulus of Silicondioxide, which is expected to be present on top of our Silicon wafer.

## 5.E Experimental Details and the Ultrasonic Amplitudes

We performed the experiments with a standard 2 N/m cantilever on a freshly cleaned Silicon sample. The sample was glued with Crystalbond 509 onto a piezo element, which has a free resonance frequency in the order of 4 MHz. In the same way, the cantilever was glued onto a similar piezo element that was mounted in a home-made cantilever holder. The cantilever and the sample were excited at 2.870 MHz and 2.871 MHz, respectively, such that both frequencies are far from any resonance of the cantilever (see Tab. 5.2 for

comparison). The experiments were performed on a Nanoscope V Multimode 8 from Veeco. We used the standard optical beam deflection method provided by this instrument to measure the motion of the cantilever. The slope of the mode shape at the cantilever's free end is proportional to the sensitivity. Since we obtain the slopes of all higher eigenmodes of the cantilever from the numerical calculations, we estimate the sensitivity, measured by the photodiode, for the $5^{th}$ mode to be 12.6 times higher than the sensitivity for the first mode. This method is valid, because the higher eigenmodes are insensitive to the tip-sample interaction such that the mode shape does not significantly change when the tip gets into contact with the sample: considering the forces applied in all experiments that are described in this thesis, we only have a maximum frequency shift of $\sim$ 10 kHz of the 5th mode at a maximum contact force $F_c = 163$ nN (see also Fig. 5.4, which shows the frequency shifts of the different modes as a function of the applied load at the free end of the cantilever in terms of the normalized tip-sample stiffness $I_1/k$). In this way, we obtained a sensitivity of 67.7 nm/V at 71.8 kHz and 5.4 nm/V at 2.87 MHz. This leads to a measured amplitude $A_t$ of the cantilever at 2.87 MHz of approximately 0.96 nm. We did not measure the amplitude $A_s$ of the sample vibration directly, which could be done with an interferometer. Instead, as the plateau in the repulsive regime depends on the amplitudes of both the cantilever $A_t$ and the sample $A_s$ (see Chap. 4 and [52]), we can estimate the sample amplitude $A_s$ to be 0.32 nm in our experiments. During the experiments we never saw the excitation $\omega_s$ of the sample in the cantilever's motion, which we attribute to the unfavorable ratio of the cantilever stiffness and the sample stiffness at MHz frequencies (see Chaps. 3 and 4 as well as [42, 52]).